A global potential energy surface and dipole moment surface for silane

Alec Owens, Sergei N. Yurchenko, Andrey Yachmenev, and Walter Thiel

Articles you may be interested in

Potential energy and dipole moment surfaces of HCO− for the search of H− in the interstellar medium
J. Chem. Phys. **136**, 224310 (2012); 10.1063/1.4724096

Calculation of the structure, potential energy surface, vibrational dynamics, and electric dipole properties for the Xe:HI van der Waals complex
J. Chem. Phys. **134**, 174302 (2011); 10.1063/1.3583817

Highly accurate potential-energy and dipole moment surfaces for vibrational state calculations of methane
J. Chem. Phys. **124**, 064311 (2006); 10.1063/1.2162891

The highly anharmonic B H 5 potential energy surface characterized in the a b initio limit
J. Chem. Phys. **122**, 104302 (2005); 10.1063/1.1853377

Quantum and classical studies of vibrational motion of CH 5 + on a global potential energy surface obtained from a novel ab initio direct dynamics approach
J. Chem. Phys. **121**, 4105 (2004); 10.1063/1.1775767

A global potential energy surface and dipole moment surface for silane

Alec Owens,[1,2,a)] Sergei N. Yurchenko,[2] Andrey Yachmenev,[2] and Walter Thiel[1]

[1]*Max-Planck-Institut für Kohlenforschung, Kaiser-Wilhelm-Platz 1, 45470 Mülheim an der Ruhr, Germany*
[2]*Department of Physics and Astronomy, University College London, Gower Street, WC1E 6BT London, United Kingdom*

A new nine-dimensional potential energy surface (PES) and dipole moment surface (DMS) for silane have been generated using high-level *ab initio* theory. The PES, CBS-F12$^{\mathrm{HL}}$, reproduces all four fundamental term values for $^{28}\mathrm{SiH}_4$ with sub-wavenumber accuracy, resulting in an overall root-mean-square error of 0.63 cm^{-1}. The PES is based on explicitly correlated coupled cluster calculations with extrapolation to the complete basis set limit, and incorporates a range of higher-level additive energy corrections to account for core-valence electron correlation, higher-order coupled cluster terms, and scalar relativistic effects. Systematic errors in computed intra-band rotational energy levels are reduced by empirically refining the equilibrium geometry. The resultant Si–H bond length is in excellent agreement with previous experimental and theoretical values. Vibrational transition moments, absolute line intensities of the v_3 band, and the infrared spectrum for $^{28}\mathrm{SiH}_4$ including states up to $J = 20$ and vibrational band origins up to 5000 cm^{-1} are calculated and compared with available experimental results. The DMS tends to marginally overestimate the strength of line intensities. Despite this, band shape and structure across the spectrum are well reproduced and show good agreement with experiment. We thus recommend the PES and DMS for future use. © 2015 AIP Publishing LLC. [http://dx.doi.org/10.1063/1.4938563]

I. INTRODUCTION

The infrared (IR) absorption spectrum of silane (SiH_4) was first documented over eighty years ago.[1,2] Since then, numerous high-resolution spectroscopic studies of SiH_4 and its isotopomers have followed, including astronomical observation of rotation-vibration transitions around the carbon star IRC +10216[3–5] and in the atmospheres of Jupiter[6] and Saturn.[7] In industry, silane gas is used extensively in the semiconductor manufacturing process and for the production of solar cells.

Despite its industrial and astrophysical importance, very few rigorous theoretical studies have been carried out. Martin, Baldridge, and Lee[8] computed an accurate quartic force field for silane based on CCSD(T) [coupled cluster with all single and double excitations and a perturbational estimate of connected triple excitations] calculations using the correlation consistent quadruple zeta basis set, cc-pVQZ,[9] plus an additional high-exponent d-function[10] (denoted as cc-pVQZ+1 in Ref. 8). Minor empirical refinement of the four diagonal quadratic constants produced a force field of spectroscopic quality (± 1 cm^{-1} when reproducing the fundamental frequencies) applicable for several isotopomers of silane.

The resultant force field was subsequently used to calculate vibrational energy levels of SiH_4, $\mathrm{SiH}_3\mathrm{D}$, SiHD_3, and $\mathrm{SiH}_2\mathrm{D}_2$ by means of canonical Van-Vleck perturbation theory (CVPT).[11] When compared to results of a variational four-dimensional stretch model, full-dimensional CVPT calculations were necessary to accurately describe certain

stretch levels as they incorporated the effects of Fermi resonance. The importance of treating Fermi interactions to compute vibrational energies of silane was also highlighted previously using an algebraic approach.[12]

The use of stretch-only models has generally been successful in describing stretching overtones[13–16] and corresponding band intensities[14,17–20] however. This is because of the pronounced local mode behaviour of silane, the effects of which have been documented experimentally in a series of papers by Zhu *et al.*[21–25] It is only at higher energies (above 12 000 cm^{-1}) that the rotational structure of the $|6000\rangle$ and $|7000\rangle$ stretch eigenstates can no longer be analysed in a local mode description due to vibrational resonances.[26] For intensity calculations, even a small treatment of bending motion can improve the description of intensities compared to stretch-only models[27] (an overview of previously computed *ab initio* dipole moment surfaces for silane can be found in Ref. 28).

The motivation for the present work is that $^{28}\mathrm{SiH}_4$ (henceforth labelled as SiH_4) is a target molecule of the ExoMol project,[29] which is creating a comprehensive database of all molecular transitions deemed necessary to model exoplanet and other hot atmospheres. Although unlikely, SiH_4 has already been considered in the context of biosignature gases on rocky exoplanets.[30]

At present, there is no coverage of SiH_4 in several of the popular spectroscopic databases.[31–34] The PNNL spectral library[35] is an exception, covering the range of 600 to 6500 cm^{-1} at a resolution of around 0.06 cm^{-1} for temperatures of 5, 25, and 50 °C. The Spherical Top Data System[36] (STDS) is another valuable resource for spectral information on silane. However, some of the measured transitions and intensities are

a)Electronic mail: owens@mpi-muelheim.mpg.de

from unpublished work which makes it hard to verify the methods used and subsequently the reliability of the data.

It is our intention to construct a global nine-dimensional potential energy surface (PES) and dipole moment surface (DMS) for silane. To do this we employ state-of-the-art electronic structure calculations to generate the respective surfaces. After fitting the *ab initio* data with suitable analytic representations, the quality of the PES and DMS will be tested by means of variational calculations of the infrared spectrum.

The paper is structured as follows: In Sec. II the *ab initio* calculations and analytic representation of the PES are presented. Similarly, in Sec. III the electronic structure calculations and analytic representation of the DMS are detailed. Pure rotational energies, the equilibrium Si–H bond length, vibrational $J = 0$ energy levels, absolute line intensities of the ν_3 band, and an overview of the rovibration spectrum up to $J = 20$ are calculated and compared against available experimental data in Sec. IV. We offer concluding remarks in Sec. V.

II. POTENTIAL ENERGY SURFACE

A. Electronic structure calculations

Focal-point analysis[37] is used to represent the total electronic energy as

$$E_{\text{tot}} = E_{\text{CBS}} + \Delta E_{\text{SR}} + \Delta E_{\text{CV}} + \Delta E_{\text{HO}}. \tag{1}$$

The energy at the complete basis set (CBS) limit E_{CBS} was computed using the explicitly correlated F12 coupled cluster method CCSD(T)-F12b (Ref. 38) with the F12-optimized correlation consistent polarized valence basis sets, cc-pVTZ-F12 and cc-pVQZ-F12.[39] Calculations were carried out in the frozen core approximation and used the diagonal fixed amplitude ansatz 3C(FIX)[40] with a Slater geminal exponent value of $\beta = 1.0\, a_0^{-1}$.[41] For the resolution of the identity (RI) basis and the two density fitting (DF) basis sets, we employed the corresponding OptRI,[42] cc-pV5Z/JKFIT,[43] and aug-cc-pwCV5Z/MP2FIT[44] auxiliary basis sets (ABS), respectively. All calculations were carried out with MOLPRO2012[45] unless stated otherwise.

A parameterized two-point formula, $E_{\text{CBS}}^C = (E_{n+1} - E_n) F_{n+1}^C + E_n$, proposed by Hill *et al.*[41] was used to extrapolate to the CBS limit. For the coefficients F_{n+1}^C, which are specific to the CCSD-F12b and (T) components of the total CCSD(T)-F12b energy, we employed values of $F^{\text{CCSD-F12b}} = 1.363\,388$ and $F^{(\text{T})} = 1.769\,474$ as recommended in Ref. 41. The Hartree-Fock (HF) energy was not extrapolated. Instead, the HF+CABS (complementary auxiliary basis set) singles correction[38] calculated in the larger basis set was used.

The scalar relativistic (SR) correction ΔE_{SR} was computed using the second-order Douglas-Kroll-Hess approach[46,47] at the CCSD(T)/cc-pVQZ-DK[48] level of theory in the frozen core approximation. The spin-orbit interaction was not considered as for light, closed-shell molecules it can be safely ignored in spectroscopic calculations.[49]

The core-valence (CV) electron correlation correction ΔE_{CV} was calculated at the CCSD(T)-F12b level of theory in conjunction with the F12-optimized correlation consistent core-valence basis set cc-pCVTZ-F12.[50] The same ansatz and ABS as in the frozen core approximation computations were used, however, we set $\beta = 1.4\, a_0^{-1}$. The $(1s)$ orbital of Si was frozen for all-electron calculations.

To estimate the higher-order (HO) correction ΔE_{HO}, we used the hierarchy of coupled cluster methods such that $\Delta E_{\text{HO}} = \Delta E_{\text{T}} + \Delta E_{(\text{Q})}$. Here the full triples contribution is $\Delta E_{\text{T}} = [E_{\text{CCSDT}} - E_{\text{CCSD(T)}}]$, and the perturbative quadruples contribution is $\Delta E_{(\text{Q})} = [E_{\text{CCSDT(Q)}} - E_{\text{CCSDT}}]$. Calculations were carried out in the frozen core approximation at the CCSD(T), CCSDT, and CCSDT(Q) levels of theory using the general coupled cluster approach[51,52] as implemented in the MRCC code[53] interfaced to CFOUR.[54] The full triples computation utilized the correlation consistent triple zeta basis set, cc-pVTZ(+d for Si),[9,55–57] whilst the perturbative quadruples computation employed the double zeta basis set, cc-pVDZ(+d for Si).

The contribution from the diagonal Born-Oppenheimer correction (DBOC) was computed with all electrons correlated (bar the $(1s)$ orbital of Si) using the CCSD method[58] as implemented in CFOUR with the aug-cc-pCVDZ basis set. A preliminary analysis of the DBOC on the vibrational energy levels showed no improvement overall when compared against experimental values. Given that inclusion of the DBOC means the PES becomes applicable only for $^{28}\text{SiH}_4$ and no other isotopologues, the correction was not included.

In generating a high-level *ab initio* PES for silane we have opted for a more pragmatic approach. Obtaining tightly converged energies with respect to basis set size for the HL corrections is less important, particularly for the CV and HO contributions which are computationally more demanding. Since the CV and HO corrections usually enter the electronic energy with opposing sign, we have calculated them together utilizing smaller basis sets. Although independently the separate corrections are not fully converged, this error is compensated for when considering their sum. This is illustrated through one-dimensional cuts of the PES in Fig. 1, most noticeably in the bending cut.

The global grid was built in terms of nine internal coordinates; four Si–H bond lengths r_1, r_2, r_3, r_4, and five $\angle(\text{H}_j–\text{Si}–\text{H}_k)$ interbond angles α_{12}, α_{13}, α_{14}, α_{23}, and α_{24}, where j and k label the respective hydrogen atoms. The Si–H stretch distances ranged from $0.98 \leq r_i \leq 2.95$ Å for $i = 1, 2, 3, 4$ whilst bending angles varied from $40 \leq \alpha_{jk} \leq 140°$ where $jk = 12, 13, 14, 23, 24$. All terms in Eq. (1) were calculated on a grid of 84 002 geometries with energies up to $hc \cdot 50\,000$ cm^{-1} (h is the Planck constant and c is the speed of light). At every grid point the coupled cluster energies were extrapolated to the CBS limit, and each HL correction was calculated and added to the total electronic energy.

The HL corrections have been computed at each grid point which is in fact time-effective at the levels of theory chosen for the electronic structure calculations. The alternative is to design reduced grids for each correction, fit a corresponding analytic representation, and apply the resulting form to the global grid of geometries by interpolation (see Refs. 59 and 60 for examples of this strategy). Although this alternative is computationally less intensive, achieving a satisfactory description of each HL correction requires careful
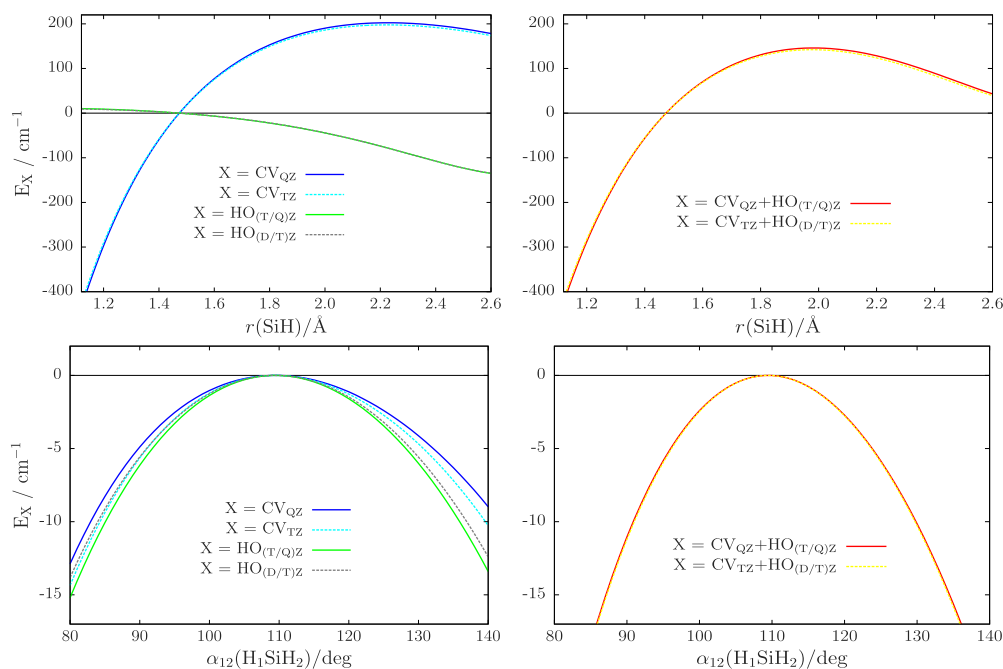
FIG. 1. One-dimensional cuts of the CV, HO, and CV+HO corrections for different sizes of basis set. For CV the subscript TZ(QZ) refers to calculations with the cc-pCVTZ-F12(cc-pCVQZ-F12) basis set. For HO the subscript (D/T)Z refers to calculations with the cc-pVDZ and cc-pVTZ basis sets for the perturbative quadruples and full triples, respectively. Likewise, the (T/Q)Z subscript corresponds to the cc-pVTZ and cc-pVQZ basis sets.

consideration and may not be trivial; any such problems are avoided in our present approach.

B. Analytic representation

The analytic representation chosen for the present study has previously been used for methane.[61–63] For the stretch coordinates,

$$\xi_i = 1 - \exp\left(-a(r_i - r^{\text{ref}})\right); \quad i = 1,2,3,4, \quad (2)$$

where $a = 1.47$ Å^{-1} and the reference equilibrium structural parameter $r^{\text{ref}} = 1.4741$ Å (value discussed in Sec. IV). The angular terms are given as symmetrized combinations of interbond angles,

$$\xi_5 = \frac{1}{\sqrt{12}}\left(2\alpha_{12} - \alpha_{13} - \alpha_{14} - \alpha_{23} - \alpha_{24} + 2\alpha_{34}\right), \quad (3)$$

$$\xi_6 = \frac{1}{2}\left(\alpha_{13} - \alpha_{14} - \alpha_{23} + \alpha_{24}\right), \quad (4)$$

$$\xi_7 = \frac{1}{\sqrt{2}}\left(\alpha_{24} - \alpha_{13}\right), \quad (5)$$

$$\xi_8 = \frac{1}{\sqrt{2}}\left(\alpha_{23} - \alpha_{14}\right), \quad (6)$$

$$\xi_9 = \frac{1}{\sqrt{2}}\left(\alpha_{34} - \alpha_{12}\right). \quad (7)$$

The potential function (maximum expansion order of $i + j + k + l + m + n + p + q + r = 6$),

$$V(\xi_1,\xi_2,\xi_3,\xi_4,\xi_5,\xi_6,\xi_7,\xi_8,\xi_9) = \sum_{ijk\ldots} \text{f}_{ijk\ldots} V_{ijk\ldots} \quad (8)$$

contains the terms

$$V_{ijk\ldots} = \{\xi_1^i \xi_2^j \xi_3^k \xi_4^l \xi_5^m \xi_6^n \xi_7^p \xi_8^q \xi_9^r\}^{T_d(M)} \quad (9)$$

which are symmetrized combinations of different permutations of the coordinates ξ_i, and transform according to the $\boldsymbol{T}_d(M)$ molecular symmetry group.[64] They are found by solving an over-determined system of linear equations in terms of the nine coordinates given above. A total of 287 symmetrically unique terms were derived up to sixth order of which only 104 were employed for the final PES. The corresponding expansion parameters $\text{f}_{ijk\ldots}$ were determined from a least-squares fitting to the *ab initio* data. Weight factors of the form[65]

$$w_i = \left(\frac{\tanh\left[-0.0006 \times (\tilde{E}_i - 15\,000)\right] + 1.002\,002\,002}{2.002\,002\,002}\right)$$
$$\times \frac{1}{N\tilde{E}_i^{(w)}} \quad (10)$$

were used in the fit. Here $\tilde{E}_i^{(w)} = \max(\tilde{E}_i, 10\,000)$, where $\tilde{E}_i$ is the potential energy at the ith geometry above equilibrium and the normalization constant $N = 0.0001$ (all values in cm^{-1}). The final fitted PES required 106 expansion parameters and employed Watson's robust fitting scheme,[66] which reduces the weights of outliers and improves the fit at lower energies. A weighted root-mean-square (rms) error of 1.77 cm^{-1} was obtained for energies up to $hc \cdot 50\,000$ cm^{-1}.

Note that geometries with $r_i \geq 2.30$ Å for $i = 1,2,3,4$ possessed a T1 diagnostic value >0.02,[67] and so the corresponding weights were reduced by several orders of magnitude. Although the coupled cluster method is not completely accurate at these points, by including them the PES maintains a reasonable shape towards dissociation. In subsequent calculations we refer to this PES as CBS-F12$^{\text{HL}}$. The CBS-F12$^{\text{HL}}$ expansion parameter set is provided in the supplementary material along with a FORTRAN routine to construct the PES.[68]

III. DIPOLE MOMENT SURFACE

A. Electronic structure calculations

The electric dipole moment is equal to the first derivative of the electronic energy with respect to external electric field strength. For each of the X, Y, and Z Cartesian coordinate axes with origin at the Si nucleus, an external electric field with components ± 0.005 a.u. was applied and the dipole moment components μ_X, μ_Y, and μ_Z computed by means of the central finite difference scheme. Calculations were carried out at the CCSD(T)/aug-cc-pVTZ(+d for Si) level of theory in the frozen core approximation using MOLPRO2012. The same nine-dimensional grid as used for the PES with energies up to $hc \cdot 50\,000$ cm^{-1} was employed.

B. Analytic representation

To represent the DMS analytically it is necessary to transform to a suitable molecule-fixed xyz coordinate system. For the present study we utilize the symmetrized molecular bond (SMB) representation for XY_4 molecules.[61] We first define unit vectors along the four Si–H bonds,

$$\mathbf{e}_i = \frac{\mathbf{r}_i - \mathbf{r}_0}{|\mathbf{r}_i - \mathbf{r}_0|}, \quad i = 1, 2, 3, 4, \quad (11)$$

where $\mathbf{r}_0$ is the position vector of the Si nucleus, and $\mathbf{r}_i$ is that of the respective H$_i$ atom. Three symmetrically independent reference vectors which span the F_2 representation are formed,

$$\mathbf{n}_1 = \frac{1}{2}(\mathbf{e}_1 - \mathbf{e}_2 + \mathbf{e}_3 - \mathbf{e}_4), \quad (12)$$

$$\mathbf{n}_2 = \frac{1}{2}(\mathbf{e}_1 - \mathbf{e}_2 - \mathbf{e}_3 + \mathbf{e}_4), \quad (13)$$

$$\mathbf{n}_3 = \frac{1}{2}(\mathbf{e}_1 + \mathbf{e}_2 - \mathbf{e}_3 - \mathbf{e}_4). \quad (14)$$

Using these the *ab initio* dipole moment vector $\boldsymbol{\mu}$ can be expressed as

$$\boldsymbol{\mu} = \mu_x \mathbf{n}_1 + \mu_y \mathbf{n}_2 + \mu_z \mathbf{n}_3. \quad (15)$$

Here, μ_α $(\alpha = x, y, z)$ are the dipole moment functions (also of F_2 symmetry) which take the form

$$\mu_\alpha(\xi_1, \xi_2, \xi_3, \xi_4, \xi_5, \xi_6, \xi_7, \xi_8, \xi_9) = \sum_{ijk\ldots} F^{(\alpha)}_{ijk\ldots} \mu^{F_2}_{\alpha, ijk\ldots}. \quad (16)$$

The expansion terms

$$\mu^{F_2}_{\alpha, ijk\ldots} = \{\xi_1^i \xi_2^j \xi_3^k \xi_4^l \xi_5^m \xi_6^n \xi_7^p \xi_8^q \xi_9^r\}^{F_{2\alpha}} \quad (17)$$

are symmetrized combinations of different permutations of coordinates ξ_i, and span the $F_{2\alpha}$ representation of the $T_d(M)$ molecular symmetry group (see Ref. 61 for more detail). A sixth order expansion was employed in terms of the coordinates,

$$\xi_i = (r_i - r^{\text{ref}}) \exp\left(-\beta(r_i - r^{\text{ref}})^2\right); \quad i = 1, 2, 3, 4 \quad (18)$$

for the stretches, with the same angular coordinates as before (Eqs. (3)–(7)). The factor $\exp\left(-\beta(r_i - r^{\text{ref}})^2\right)$ prevents the expansion from diverging at large values of r_i. Our DMS fitting employed the parameters $r^{\text{ref}} = 1.5355$ Å and $\beta = 1.0$ Å^{-2}.

The expansion coefficients $F^{(\alpha)}_{ijk\ldots}$ for all three components $\alpha = x, y, z$ were determined simultaneously through a least squares fitting to the *ab initio* data. Again weight factors of the form given in Eq. (10) were used which favor energies below $hc \cdot 15\,000$ cm^{-1}. The fitting required 283 parameters and reproduced the *ab initio* data with a weighted rms error of 0.001 D for energies up to $hc \cdot 50\,000$ cm^{-1}. The expansion parameter set for the DMS is provided in the supplementary material along with a FORTRAN routine to construct the corresponding analytic representation.[68]

IV. RESULTS

A. Equilibrium bond length and pure rotational energies

Since rotational energies are highly dependent on the molecular geometry through the moments of inertia, we first refine the Si–H reference equilibrium structural parameter r^{ref} before we proceed to extensive rovibrational energy level calculations. Thereby, the accuracy of the computed intra-band rotational wavenumbers can be significantly improved.[69,70]

Two iterations of a nonlinear least-squares fit to the experimental $J \leq 6$ rotational energies from Ref. 36 produced a refined parameter of $r^{\text{ref}} = 1.4741$ Å. However, due to the inclusion of a linear expansion term in the parameter set of our potential, this value does not define the minimum of the PES. The true equilibrium bond length was determined to be $r^{\text{eq}} = 1.4737$ Å. This is in good agreement with the experimental estimate of $r(\text{Si–H}) = 1.4741$ Å,[71] and an *ab initio* value of $r(\text{Si–H}) = 1.4742$ Å calculated at the all

TABLE I. Comparison of calculated and experimental $J \leq 6$ pure rotational term values (in cm^{-1}) for ^{28}SiH$_4$. The observed ground state energy levels are from Ref. 36.

J	K	Symmetry	Experiment	Calculated	Obs−calc
0	0	A_1	0.000 00	0.000 00	0.000 00
1	1	F_1	5.718 01	5.718 00	0.000 01
2	2	E	17.153 06	17.153 02	0.000 04
2	1	F_2	17.153 21	17.153 17	0.000 04
3	2	A_2	34.304 53	34.304 48	0.000 05
3	3	F_1	34.303 19	34.303 13	0.000 06
3	1	F_2	34.303 79	34.303 73	0.000 06
4	0	A_1	57.164 74	57.164 67	0.000 07
4	2	E	57.166 53	57.166 47	0.000 06
4	1	F_1	57.165 78	57.165 72	0.000 06
4	3	F_2	57.168 77	57.168 72	0.000 05
5	2	E	85.742 33	85.742 31	0.000 02
5	1	F_1	85.735 10	85.735 04	0.000 06
5	3	F_1	85.743 30	85.743 28	0.000 02
5	5	F_2	85.737 11	85.737 07	0.000 04
6	4	A_1	120.025 74	120.025 81	−0.000 07
6	2	A_2	120.011 43	120.011 44	−0.000 01
6	6	E	120.007 84	120.007 84	0.000 00
6	3	F_1	120.023 50	120.023 56	−0.000 06
6	1	F_2	120.008 73	120.008 74	−0.000 01
6	5	F_2	120.020 97	120.021 02	−0.000 05

electron CCSD(T)/cc-pCVQZ level of theory.[72] Note that before the refinement the original *ab initio* bond length of the CBS-F12^{HL} PES was $r^{eq}_{ab\ initio}$ = 1.4735 Å.

The computed pure rotational energies are listed in Table I. The details of the calculations will be discussed in Sec. IV B. As can be seen, the agreement with experiment is excellent and energy levels up to $J \leq 6$ are reproduced with a rms error of 0.000 05 cm^{-1}. We therefore expect the true Si–H equilibrium bond length to be very close to the value r^{eq} = 1.4737 Å.

TABLE II. Comparison of calculated and experimental $J = 0$ vibrational term values (in cm^{-1}) for ^{28}SiH$_4$. The zero-point energy was computed to be 6847.084 cm^{-1}.

Mode	Symmetry	Experiment	Calculated	Obs−calc	Reference
ν_4	F_2	913.47	912.85	0.62	36
ν_2	E	970.93	970.14	0.79	36
$2\nu_4$	A_1	1811.80	1810.90	0.90	36
$2\nu_4$	F_2	1824.19	1823.15	1.04	36
$2\nu_4$	E	1827.81	1827.00	0.81	36
$\nu_2+\nu_4$	F_2	1881.96	1880.87	1.09	36
$\nu_2+\nu_4$	F_1	1887.10	1885.36	1.74	36
$2\nu_2$	A_1	1937.50	1935.84	1.66	36
$2\nu_2$	E	1942.77	1941.29	1.48	36
ν_1	A_1	2186.87	2187.63	−0.76	36
ν_3	F_2	2189.19	2189.32	−0.13	36
$3\nu_4$	F_2	2713.07	2712.16	0.91	36
$3\nu_4$	A_1	2731.17	2729.97	1.20	36
$3\nu_4$	F_1	2735.42	2734.26	1.16	36
$3\nu_4$	F_2	2739.35	2738.48	0.87	36
$\nu_2+2\nu_4$	E	2780.47	2779.32	1.15	36
$\nu_2+2\nu_4$	F_1	2793.32	2791.84	1.48	36
$\nu_2+2\nu_4$	A_1	2795.11	2793.94	1.17	36
$\nu_2+2\nu_4$	F_2	2797.41	2795.53	1.88	36
$\nu_2+2\nu_4$	E	2800.20	2798.25	1.95	36
$\nu_2+2\nu_4$	A_2	2803.95	2801.56	2.39	36
$2\nu_2+\nu_4$	F_2	2848.26	2846.60	1.66	36
$2\nu_2+\nu_4$	F_1	2856.43	2854.36	2.07	36
$2\nu_2+\nu_4$	F_2	2859.74	2857.18	2.56	36
$3\nu_2$	E	2904.99	2902.60	2.39	36
$3\nu_2$	A_1	2915.40	2913.34	2.06	36
$3\nu_2$	A_2	2915.48	2913.44	2.04	36
$\nu_3+\nu_4$	F_1	3094.81	3094.35	0.46	11[a]
$\nu_1+\nu_4$	F_2	3095.26	3095.10	0.16	11[a]
$\nu_3+\nu_4$	E	3095.86	3095.52	0.34	11[a]
$\nu_3+\nu_4$	F_2	3098.02	3097.60	0.42	11[a]
$\nu_3+\nu_4$	A_1	3099.48	3098.73	0.75	11[a]
$\nu_2+\nu_3$	F_2	3152.59	3152.92	−0.33	11[a]
$\nu_2+\nu_3$	F_1	3153.08	3152.17	0.91	11[a]
$\nu_1+\nu_2$	E	3153.60	3152.12	1.48	11[a]
$2\nu_3$	A_1	4308.87	4308.96	−0.09	26[b]
$\nu_1+\nu_3$	F_2	4309.35	4309.89	−0.54	24
$2\nu_1$	A_1	4374.56	4375.92	−1.36	15[c]
$2\nu_3$	E	4378.40	4380.23	−1.83	36
$2\nu_3$	F_2	4380.28	4378.73	1.55	15[c]
$\nu_1+2\nu_3$	A_1	6362.05	6362.88	−0.83	26[d]
$3\nu_3$	F_2	6362.05	6362.97	−0.92	26[d]
$3\nu_1$	A_1	6496.13	6498.19	−2.06	15[c]
$2\nu_1+\nu_3$	F_2	6497.45	6498.48	−1.03	25
$\nu_1+2\nu_3$	E	6500.30	6500.58	−0.28	15[c]
$3\nu_3$	F_2	6500.60	6500.71	−0.11	15[c]
$3\nu_3$	F_1	6502.88	6502.94	−0.06	15[c]
$\nu_1+3\nu_3$	A_1	8347.86	8349.38	−1.52	26[d]
$\nu_1+3\nu_3$	F_2	8347.86	8349.39	−1.53	26[d]

[a]Originally attributed to Ref. 36, but unable to confirm value independently.
[b]Originally attributed to Ref. 24.
[c]Originally attributed to Ref. 78.
[d]Originally attributed to Refs. 21–23.

B. Vibrational $J = 0$ energies

To calculate rovibrational energy levels, transition frequencies and corresponding intensities, we use the variational nuclear motion code TROVE.[73] Here we only summarize the key aspects of our calculations. Details of the general methodology can be found in Refs. 69, 73, and 74.

The rovibrational Hamiltonian was represented as a power series expansion around the equilibrium geometry in terms of the coordinates given in Eqs. (2)–(7), and was constructed numerically using an automatic differentiation method.[74] The kinetic and potential energy operators were truncated at 6th and 8th order, respectively, which is sufficient for our purposes. For a discussion of the associated errors of such a scheme see Refs. 73 and 74. Note that atomic mass values were employed in the subsequent TROVE calculations.

The vibrational basis set was generated using a multi-step contraction scheme. For SiH_4 the polyad number

$$P = 2(n_1 + n_2 + n_3 + n_4) + n_5 + n_6 + n_7 + n_8 + n_9 \leq P_{max} \tag{19}$$

controls the size of the basis set and does not exceed a predefined maximum value P_{max}. For $J = 0$ vibrational energy level calculations we set $P_{max} = 14$. Here the quantum numbers n_k for $k = 1, \ldots, 9$ correspond to primitive basis functions ϕ_{n_k}, which are obtained by solving a one-dimensional Schrödinger equation for each vibrational mode by means of the Numerov-Cooley method.[75,76]

The normal modes of silane are classified by the symmetry species, A_1, E, and F_2. Of A_1 symmetry is the non-degenerate symmetric stretching mode ν_1 (2186.87 cm^{-1}). The doubly degenerate asymmetric bending mode ν_2 (970.93 cm^{-1}) has E symmetry. Whilst of F_2 symmetry are the triply degenerate modes; the asymmetric stretching mode ν_3 (2189.19 cm^{-1}), and the asymmetric bending mode ν_4 (913.47 cm^{-1}). The values in parentheses are the experimentally determined values from Ref. 36. To be of spectroscopic use we map the vibrational quantum numbers n_k of TROVE to the normal mode quantum numbers v_k commonly used. For SiH_4 the vibrational states are labelled as $v_1\nu_1 + v_2\nu_2 + v_3\nu_3 + v_4\nu_4$ where v_i counts the level of excitation.

In Table II the computed vibrational energies using the CBS-F12^{HL} PES are listed against all available experimental data up to 8500 cm^{-1}. The four fundamental frequencies are all reproduced with sub-wavenumber accuracy, resulting in an overall rms error of 0.63 cm^{-1} and a mean-absolute-deviation (mad) of 0.57 cm^{-1}. Altogether, the 49 experimental levels

are reproduced with a rms error of 1.33 cm^{-1} and mad of 1.07 cm^{-1}. Note that energies are converged to 0.01 cm^{-1} or better (the majority are converged to orders of magnitude lower), except for the two levels at 8347.86 cm^{-1} which are converged to within 0.02 cm^{-1}. This was confirmed by performing a complete vibrational basis set extrapolation with values of $P_{max} = \{10, 12, 14\}$ (see Refs. 60 and 77 for further details).

Of the 35 term values up to 3153.60 cm^{-1}, the energy of 32 levels is underestimated by the CBS-F12^{HL} PES. This can be explained by the residual errors of the ν_2 and ν_4 fundamentals, which largely dictates the accuracy of the subsequent combination bands and overtones. Above 3153.60 cm^{-1}, computed energy levels are consistently higher than experiment which is a result of overestimating the ν_1 and ν_3 fundamentals. Despite this, the performance of the CBS-F12^{HL} PES is extremely encouraging, especially considering that for vibrational $J = 0$ energy levels the PES can be regarded as an *ab initio* surface.

Experimental values for stretching overtones above 8500 cm^{-1} are available.[22,26,79] However, the corresponding values in TROVE are harder to identify given the increased density of states at higher energies. Highly excited modes also show slower convergence with respect to vibrational basis set size. Thus, to obtain reasonably well converged energies would require calculations with $P_{max} = 16$ or greater, which is currently unachievable with the computational resources available to us.

As an aside in Table III, we show the effect of the empirical refinement of the equilibrium geometry on the fundamental frequencies. Results computed using the *ab initio* bond length (overall rms error of 0.57 cm^{-1}) are marginally better which is to be expected. In the refined geometry PES the shape of the original *ab initio* PES has been altered by shifting its minimum, resulting in a poorer representation of vibrational energies. For spectral analysis an improved description of rotational structure is more desirable however, as vibrational band position can be easily corrected at a later stage.[69]

C. Vibrational transition moments

The vibrational transition moment is defined as

$$\mu_{if} = \sqrt{\sum_{\alpha=x,y,z} |\langle \Phi_{vib}^{(f)} | \bar{\mu}_\alpha | \Phi_{vib}^{(i)} \rangle|^2}, \tag{20}$$

where $|\Phi_{vib}^{(i)}\rangle$ and $|\Phi_{vib}^{(f)}\rangle$ are the initial and final state vibrational eigenfunctions, respectively, and $\bar{\mu}_\alpha$ is the electronically

TABLE III. Comparison of the computed fundamental term values (in cm^{-1}) with the refined and *ab initio* equilibrium geometry.

Mode	Symmetry	Experiment[a]	Refined equilibrium (A)	*Ab initio* equilibrium (B)	Obs-calc (A)	Obs-calc (B)
ν_1	A_1	2186.87	2187.63	2187.63	−0.76	−0.76
ν_2	E	970.93	970.14	970.26	0.79	0.67
ν_3	F_2	2189.19	2189.32	2189.31	−0.13	−0.12
ν_4	F_2	913.47	912.85	912.97	0.62	0.50

[a]See Table II for experimental references.

TABLE IV. Calculated vibrational transition moments (in D) and frequencies (in cm^{-1}) from the vibrational ground state for ^{28}SiH$_4$. Only levels of F_2 symmetry are accessible from the ground state in IR absorption.

Mode	Symmetry	Experiment[a]	Calculated	μ_{if}
ν_4	F_2	913.47	912.85	0.4149×10^0
$2\nu_4$	F_2	1824.19	1823.15	0.2500×10^{-2}
$\nu_2 + \nu_4$	F_2	1881.96	1880.87	0.2350×10^{-1}
ν_3	F_2	2189.19	2189.32	0.2470×10^0
$3\nu_4$	F_2	2713.07	2712.16	0.4578×10^{-2}
$3\nu_4$	F_2	2739.35	2738.48	0.8123×10^{-3}
$\nu_2 + 2\nu_4$	F_2	2797.41	2795.53	0.1734×10^{-2}
$2\nu_2 + \nu_4$	F_2	2848.26	2846.60	0.1835×10^{-2}
$2\nu_2 + \nu_4$	F_2	2859.74	2857.18	0.9093×10^{-4}
$\nu_1 + \nu_4$	F_2	3095.26	3095.10	0.1320×10^{-1}
$\nu_3 + \nu_4$	F_2	3098.02	3097.60	0.1319×10^{-1}
$\nu_2 + \nu_3$	F_2	3152.59	3152.92	0.1050×10^{-1}
$4\nu_4$	F_2	...	3609.08	0.4741×10^{-3}
$4\nu_4$	F_2	...	3638.92	0.1892×10^{-4}
$\nu_2 + 3\nu_4$	F_2	...	3677.72	0.6075×10^{-3}
$\nu_2 + 3\nu_4$	F_2	...	3704.01	0.5424×10^{-3}
$\nu_2 + 3\nu_4$	F_2	...	3707.66	0.2098×10^{-4}
$2\nu_2 + 2\nu_4$	F_2	...	3758.50	0.1628×10^{-3}
$2\nu_2 + 2\nu_4$	F_2	...	3767.13	0.5799×10^{-4}
$3\nu_2 + \nu_4$	F_2	...	3810.86	0.2432×10^{-3}
$3\nu_2 + \nu_4$	F_2	...	3827.61	0.3848×10^{-3}
$\nu_1 + \nu_3$	F_2	4309.35	4309.89	0.1336×10^{-1}
$2\nu_3$	F_2	4380.28	4378.73	0.4262×10^{-2}
$3\nu_3$	F_2	6362.05	6362.97	0.5762×10^{-3}
$2\nu_1 + \nu_3$	F_2	6497.45	6498.48	0.5813×10^{-3}
$3\nu_3$	F_2	6500.60	6500.71	0.1517×10^{-3}
$\nu_1 + 3\nu_3$	F_2	8347.86	8349.39	0.1390×10^{-2}

[a]See Table II for experimental references.

averaged dipole moment function along the molecule-fixed axis $\alpha = x, y, z$. In Table IV we list computed vibrational transition moments from the vibrational ground state. Calculations used the CBS-F12^{HL} PES and a polyad number of $P_{max} = 12$ which ensured converged results.

Experimentally determined transition moments have only been derived for the ν_3 (2189.19 cm^{-1}) and ν_4 (913.47 cm^{-1}) modes. Fox and Person[80] using earlier band intensity measurements[81,82] found $\mu_{\nu_3} = 0.139 \pm 4\%$ D and $\mu_{\nu_4} = 0.232 \pm 7\%$ D. The reliability of the intensity data[81,82] has, however, been questioned.[83] In other work, Cadot[84] determined a transition moment of $\mu_{\nu_3} = 0.1293 \pm 3\%$ D. Whilst a value of $\mu_{\nu_4} = 0.247$ D was quoted in Ref. 4 but attributed to unpublished results.

Although the experimental situation is not entirely clear, the computed TROVE transition moments of $\mu_{\nu_3} = 0.2470$ D and $\mu_{\nu_4} = 0.4149$ D are notably larger than their experimental counterparts. We will show in Secs. IV D and IV E that our DMS does marginally overestimate the strength of line intensities. The magnitude of this overestimation is not consistent with the discrepancy in the experimental and computed values for μ_{ν_3} and μ_{ν_4} however. Experimentally derived transition moments for the other levels of silane could help clarify previous results and assist future theoretical benchmarking.

It is worth nothing that if we use the values from Ref. 80 and compare the ratio $\mu_{\nu_3}^{exp}/\mu_{\nu_4}^{exp} = 0.599$ with $\mu_{\nu_3}^{TROVE}/\mu_{\nu_4}^{TROVE} = 0.595$, there is excellent agreement which suggests our relative intensity for the two strongest bands is reasonable.

D. Absolute line intensities of the ν_3 band

To simulate absolute absorption intensities we use the expression

$$I(f \leftarrow i) = \frac{A_{if}}{8\pi c} g_{ns}(2J_f + 1)\frac{\exp(-E_i/kT)}{Q(T)\,\nu_{if}^2}$$
$$\times \left[1 - \exp\left(-\frac{hc\nu_{if}}{kT}\right)\right], \qquad (21)$$

where A_{if} is the Einstein-A coefficient of a transition with frequency ν_{if} between an initial state with energy E_i, and a final state with rotational quantum number J_f. Here k is the Boltzmann constant, T is the absolute temperature, and c is the speed of light. The nuclear spin statistical weights are $g_{ns} = \{5, 5, 2, 3, 3\}$ for states of symmetry $\{A_1, A_2, E, F_1, F_2\}$, respectively. The partition function $Q(T)$ was estimated using $Q(T) \approx Q_{rot}(T) \times Q_{vib}(T)$. For tetrahedral molecules the rotational partition function is given as[85]

$$Q_{rot}(T) = \frac{4}{3}\pi^{1/2}\left(\frac{Bhc}{kT}\right)^{-3/2}\exp\left(\frac{Bhc}{4kT}\right), \qquad (22)$$

where for SiH$_4$ we use a ground state rotational constant of $B = 2.859$, which is consistent with Refs. 86–88. At $T = 296$ K, $Q_{rot} = 1447.6001$, the vibrational partition function $Q_{vib} = 1.0551$,[36] resulting in $Q = 1527.3629$.

A recent high-resolution study of the ν_3 band measured the absolute line intensities of numerous P-branch transitions up to $J = 16$ at 296 K.[89] Line intensities were recorded at a resolution of 0.0011 cm^{-1} and were given an estimated experimental measurement accuracy of 10%. To validate our DMS and to a lesser extent the PES, in Table V we compare frequencies and absolute line intensities of over 100 transitions from Ref. 89. The results are also illustrated in Fig. 2.

Due to the computational demands of calculating higher rotational excitation (rovibrational matrices scale linearly with J), calculations were performed with $P_{max} = 10$. Convergence tests were carried out up to $J = 6$ for $P_{max} = 12$. The corresponding transition frequencies showed a consistent correction of around $\Delta(P_{max} = 12) = -0.00185$ cm^{-1}. This correction was applied to all computed frequencies listed in Table V. For the corresponding intensities, the $1 \leftarrow 2$ ($J' \leftarrow J''$) transitions possessed a convergence correction of the order 10^{-24}. The magnitude of this correction showed a linear relationship with increasing J, from which we estimate that for the $15 \leftarrow 16$ transitions the correction would be of the order 10^{-22}. The respective intensities therefore have an error of at most 1%. We are confident that the results in Table V are sufficiently converged to reliably evaluate the DMS and PES.

Around one third of the calculated absolute line intensities are within the estimated experimental measurement accuracy

TABLE V. Comparison of calculated and observed frequencies (in cm^{-1}) and absolute line intensities (in cm/molecule) for transitions between the ν_3 and ground vibrational state. To quantify the error in the computed line intensity we use the percentage measure, $\%[(\text{obs}-\text{calc})/\text{obs}]$.

Γ'	J'	K'	Γ''	J''	K''	ν_{obs}	ν_{calc}	$\Delta_{\text{obs}-\text{calc}}$	I_{obs}	I_{calc}	$\%\left[\frac{\text{obs}-\text{calc}}{\text{obs}}\right]$
F_1	1	1	F_2	2	1	2177.782	2177.908	−0.126	8.784×10^{-20}	1.005×10^{-19}	−14.42
E	1	1	E	2	1	2177.793	2177.921	−0.128	5.920×10^{-20}	6.701×10^{-20}	−13.19
A_1	2	1	A_2	3	1	2172.045	2172.170	−0.125	2.290×10^{-19}	2.586×10^{-19}	−12.92
F_1	2	1	F_2	3	1	2172.072	2172.197	−0.125	1.417×10^{-19}	1.535×10^{-19}	−8.38
F_2	2	1	F_1	3	2	2172.091	2172.216	−0.125	1.315×10^{-19}	1.550×10^{-19}	−17.88
F_1	3	1	F_2	4	2	2166.306	2166.431	−0.125	1.682×10^{-19}	1.889×10^{-19}	−12.35
E	3	1	E	4	1	2166.340	2166.466	−0.126	1.212×10^{-19}	1.301×10^{-19}	−7.37
F_2	3	2	F_1	4	1	2166.357	2166.483	−0.126	1.776×10^{-19}	1.935×10^{-19}	−8.98
A_2	3	2	A_1	4	0	2166.377	2166.504	−0.127	2.923×10^{-19}	3.250×10^{-19}	−11.17
F_2	4	2	F_1	5	2	2160.524	2160.654	−0.130	1.959×10^{-19}	2.118×10^{-19}	−8.09
E	4	2	E	5	1	2160.547	2160.678	−0.131	1.270×10^{-19}	1.361×10^{-19}	−7.16
F_1	4	1	F_2	5	3	2160.591	2160.718	−0.127	2.201×10^{-19}	2.191×10^{-19}	0.44
F_2	4	1	F_1	5	1	2160.629	2160.755	−0.126	2.250×10^{-19}	2.150×10^{-19}	4.43
A_2	5	2	A_1	6	2	2154.706	2154.832	−0.126	3.217×10^{-19}	3.766×10^{-19}	−17.08
F_2	5	2	F_1	6	2	2154.738	2154.865	−0.127	1.930×10^{-19}	2.135×10^{-19}	−10.62
F_1	5	1	F_2	6	3	2154.768	2154.895	−0.127	1.852×10^{-19}	1.939×10^{-19}	−4.70
F_1	5	1	F_2	6	1	2154.780	2154.907	−0.127	1.705×10^{-20}	2.058×10^{-20}	−20.73
A_1	5	3	A_2	6	1	2154.810	2154.935	−0.125	3.688×10^{-19}	3.826×10^{-19}	−3.73
F_1	5	1	F_2	6	3	2154.844	2154.975	−0.131	1.071×10^{-20}	1.491×10^{-20}	−39.28
F_1	5	1	F_2	6	1	2154.856	2154.987	−0.131	1.901×10^{-19}	2.039×10^{-19}	−7.29
E	5	1	E	6	3	2154.862	2154.992	−0.130	1.380×10^{-19}	1.485×10^{-19}	−7.60
F_2	6	2	F_1	7	3	2148.893	2149.021	−0.128	1.970×10^{-19}	2.025×10^{-19}	−2.77
E	6	2	E	7	3	2148.926	2149.052	−0.126	1.319×10^{-19}	1.400×10^{-19}	−6.17
F_1	6	3	F_2	7	2	2148.954	2149.080	−0.126	1.639×10^{-19}	1.702×10^{-19}	−3.89
F_1	6	3	F_2	7	1	2148.976	2149.102	−0.126	3.234×10^{-20}	4.017×10^{-20}	−24.23
A_1	6	3	A_2	7	1	2149.046	2149.184	−0.138	2.950×10^{-19}	3.153×10^{-19}	−6.89
F_1	6	1	F_2	7	2	2149.052	2149.186	−0.134	2.740×10^{-20}	2.832×10^{-20}	−3.34
F_1	6	1	F_2	7	1	2149.074	2149.207	−0.133	1.714×10^{-19}	1.781×10^{-19}	−3.88
F_2	6	3	F_1	7	1	2149.082	2149.214	−0.132	2.077×10^{-19}	2.140×10^{-19}	−3.02
F_1	7	3	F_2	8	2	2143.025	2143.165	−0.140	1.747×10^{-19}	1.899×10^{-19}	−8.70
E	7	3	E	8	1	2143.056	2143.197	−0.141	9.223×10^{-20}	1.032×10^{-19}	−11.94
F_2	7	2	F_1	8	2	2143.084	2143.223	−0.139	1.740×10^{-19}	1.798×10^{-19}	−3.30
E	7	3	E	8	3	2143.104	2143.246	−0.142	1.340×10^{-20}	2.002×10^{-20}	−49.38
F_2	7	2	F_1	8	1	2143.125	2143.264	−0.139	1.201×10^{-20}	1.525×10^{-20}	−26.99
E	7	1	E	8	1	2143.228	2143.372	−0.144	6.575×10^{-21}	1.017×10^{-20}	−54.68
A_2	7	1	A_1	8	0	2143.286	2143.424	−0.138	3.771×10^{-19}	3.373×10^{-19}	10.56
F_1	8	3	F_2	9	1	2137.100	2137.240	−0.140	1.135×10^{-20}	1.265×10^{-20}	−11.48
A_1	8	3	A_2	9	3	2137.136	2137.267	−0.131	2.554×10^{-19}	2.951×10^{-19}	−15.55
F_1	8	2	F_2	9	3	2137.173	2137.301	−0.128	1.546×10^{-19}	1.452×10^{-19}	6.09
F_2	8	2	F_1	9	4	2137.198	2137.324	−0.126	1.010×10^{-19}	1.313×10^{-19}	−29.97
F_2	8	2	F_1	9	4	2137.417	2137.570	−0.153	1.122×10^{-20}	1.493×10^{-20}	−33.10
F_2	8	1	F_1	9	2	2137.426	2137.569	−0.143	3.185×10^{-21}	3.613×10^{-21}	−13.46
E	9	3	E	10	3	2131.274	2131.402	−0.128	8.116×10^{-20}	8.571×10^{-20}	−5.61
F_2	9	4	F_1	10	3	2131.298	2131.424	−0.126	9.629×10^{-20}	1.082×10^{-19}	−12.38
A_1	9	1	A_2	10	1	2131.302	2131.439	−0.137	4.663×10^{-20}	6.417×10^{-20}	−37.62
F_1	9	3	F_2	10	2	2131.315	2131.445	−0.130	5.899×10^{-21}	7.399×10^{-21}	−25.42
F_2	9	4	F_1	10	1	2131.340	2131.467	−0.127	2.822×10^{-20}	3.382×10^{-20}	−19.86
F_1	9	3	F_2	10	1	2131.381	2131.512	−0.131	1.117×10^{-20}	1.499×10^{-20}	−34.22
E	9	3	E	10	5	2131.399	2131.527	−0.128	6.337×10^{-21}	9.306×10^{-21}	−46.85
F_1	9	1	F_2	10	4	2131.594	2131.678	−0.084	6.694×10^{-21}	3.753×10^{-21}	43.93
F_2	9	3	F_1	10	3	2131.600	2131.764	−0.164	1.449×10^{-20}	1.615×10^{-20}	−11.48
A_2	9	4	A_1	10	4	2131.629	2131.796	−0.167	1.534×10^{-19}	1.616×10^{-19}	−5.31
A_1	9	3	A_2	10	1	2131.672	2131.826	−0.154	1.876×10^{-19}	1.952×10^{-19}	−4.06
F_2	10	4	F_1	11	2	2125.142	2125.281	−0.139	1.315×10^{-20}	1.212×10^{-20}	7.82
E	10	1	E	11	3	2125.162	2125.302	−0.140	2.551×10^{-20}	2.212×10^{-20}	13.30
F_2	10	4	F_1	11	4	2125.194	2125.333	−0.139	1.512×10^{-20}	1.610×10^{-20}	−6.46
E	10	1	E	11	1	2125.249	2125.389	−0.140	8.867×10^{-21}	1.032×10^{-20}	−16.41
F_2	10	4	F_1	11	2	2125.312	2125.441	−0.129	1.016×10^{-19}	1.011×10^{-19}	0.58
E	10	2	E	11	3	2125.340	2125.467	−0.127	5.186×10^{-20}	5.236×10^{-20}	−0.97

TABLE V. (*Continued.*)

Γ'	J'	K'	Γ''	J''	K''	ν_{obs}	ν_{calc}	$\Delta_{obs-calc}$	I_{obs}	I_{calc}	$\%\left[\frac{obs-calc}{obs}\right]$
F_1	10	1	F_2	11	2	2125.348	2125.481	−0.133	1.369×10^{-20}	1.531×10^{-20}	−11.88
F_1	10	3	F_2	11	3	2125.362	2125.488	−0.126	9.684×10^{-20}	1.020×10^{-19}	−5.32
A_1	10	4	A_2	11	1	2125.809	2125.973	−0.164	1.579×10^{-19}	1.712×10^{-19}	−8.44
E	10	4	E	11	1	2125.851	2126.025	−0.174	3.963×10^{-20}	4.194×10^{-20}	−5.82
F_2	11	1	F_1	12	4	2119.300	2119.431	−0.131	9.978×10^{-21}	1.400×10^{-20}	−40.30
A_2	11	2	A_1	12	4	2119.331	2119.461	−0.130	1.160×10^{-19}	1.440×10^{-19}	−24.15
F_1	11	3	F_2	12	5	2119.389	2119.515	−0.126	6.041×10^{-20}	6.883×10^{-20}	−13.94
A_1	11	3	A_2	12	3	2119.414	2119.540	−0.126	1.131×10^{-19}	1.477×10^{-19}	−30.63
F_2	11	1	F_1	12	2	2119.440	2119.571	−0.131	1.284×10^{-20}	1.634×10^{-20}	−27.32
F_1	11	3	F_2	12	1	2119.449	2119.576	−0.127	7.866×10^{-21}	1.017×10^{-20}	−29.29
F_2	11	2	F_1	12	2	2119.508	2119.635	−0.127	1.635×10^{-20}	2.204×10^{-20}	−34.82
F_2	12	1	F_1	13	1	2114.154	2114.321	−0.167	4.479×10^{-20}	5.868×10^{-20}	−31.03
E	12	5	E	13	1	2114.169	2114.352	−0.183	2.707×10^{-20}	3.394×10^{-20}	−25.38
F_1	12	1	F_2	13	1	2114.179	2114.349	−0.170	4.882×10^{-20}	5.374×10^{-20}	−10.08
F_2	12	1	F_1	13	2	2114.187	2114.373	−0.186	3.173×10^{-20}	4.001×10^{-20}	−26.09
A_1	12	1	A_2	13	5	2114.252	2114.453	−0.201	4.283×10^{-20}	5.208×10^{-20}	−21.59
F_2	12	3	F_1	13	5	2114.259	2114.457	−0.198	2.253×10^{-20}	2.647×10^{-20}	−17.51
F_1	12	4	F_2	13	1	2114.263	2114.463	−0.200	2.538×10^{-20}	2.854×10^{-20}	−12.45
A_2	12	4	A_1	13	2	2114.309	2114.506	−0.197	3.990×10^{-20}	4.713×10^{-20}	−18.13
F_2	12	3	F_1	13	2	2114.354	2114.554	−0.200	2.886×10^{-21}	3.277×10^{-21}	−13.55
E	13	2	E	14	7	2108.308	2108.486	−0.178	2.272×10^{-20}	2.725×10^{-20}	−19.96
F_1	13	1	F_2	14	1	2108.321	2108.499	−0.178	3.210×10^{-20}	3.888×10^{-20}	−21.14
A_2	13	5	A_1	14	6	2108.343	2108.545	−0.202	5.088×10^{-20}	5.941×10^{-20}	−16.77
F_1	13	2	F_2	14	2	2108.349	2108.544	−0.195	2.889×10^{-20}	3.389×10^{-20}	−17.30
A_1	13	2	A_2	14	1	2108.354	2108.535	−0.181	5.234×10^{-20}	5.969×10^{-20}	−14.04
F_2	13	2	F_1	14	3	2108.392	2108.590	−0.198	2.090×10^{-20}	2.445×10^{-20}	−17.00
F_1	13	2	F_2	14	5	2108.482	2108.694	−0.212	1.629×10^{-20}	1.955×10^{-20}	−20.03
F_2	13	3	F_1	14	1	2108.501	2108.711	−0.210	1.259×10^{-20}	1.537×10^{-20}	−22.06
E	13	4	E	14	3	2108.510	2108.721	−0.211	9.767×10^{-21}	1.165×10^{-20}	−19.31
A_1	14	3	A_2	15	5	2101.289	2101.420	−0.131	5.038×10^{-20}	5.580×10^{-20}	−10.74
F_1	14	4	F_2	15	4	2101.294	2101.420	−0.126	9.089×10^{-21}	7.565×10^{-21}	16.77
F_2	14	2	F_1	15	2	2101.310	2101.440	−0.130	5.713×10^{-21}	6.863×10^{-21}	−20.13
F_1	14	3	F_2	15	4	2101.345	2101.472	−0.127	1.368×10^{-20}	1.974×10^{-20}	−44.37
F_2	14	5	F_1	15	4	2101.369	2101.496	−0.127	2.202×10^{-20}	2.588×10^{-20}	−17.52
A_2	14	4	A_1	15	4	2101.397	2101.523	−0.126	3.615×10^{-20}	5.131×10^{-20}	−41.95
E	14	2	E	15	1	2101.445	2101.569	−0.124	2.451×10^{-21}	3.595×10^{-21}	−46.67
A_2	15	4	A_1	16	0	2096.608	2096.799	−0.191	2.530×10^{-20}	3.021×10^{-20}	−19.42
E	15	2	E	16	1	2096.658	2096.850	−0.192	9.113×10^{-21}	1.064×10^{-20}	−16.71
F_1	15	2	F_2	16	3	2096.686	2096.897	−0.211	1.131×10^{-20}	1.532×10^{-20}	−35.38
E	15	6	E	16	7	2096.743	2096.963	−0.220	8.317×10^{-21}	9.454×10^{-21}	−13.67
F_1	15	3	F_2	16	1	2096.772	2096.994	−0.222	9.262×10^{-21}	1.085×10^{-20}	−17.14
F_2	15	7	F_1	16	2	2096.802	2097.017	−0.215	9.495×10^{-21}	1.206×10^{-20}	−26.98

of 10%. However, as is best seen by the residuals plotted in Fig. 2, nearly all of the computed line intensities are larger than the corresponding experimental values. We suspect this is due to the electronic structure calculations and the use of only a triple-zeta basis set, aug-cc-pVTZ(+d for Si), to generate the DMS. A larger (augmented) correlation consistent basis set and possibly the inclusion of additional higher-level corrections (such as those incorporated for the PES) would most likely reduce the strength of computed line intensities. Despite this, Fig. 2 shows that the ν_3 band is well reproduced. Computed frequencies are on average larger by 0.1–0.2 cm^{-1} across all transitions. This more or less systematic error can be attributed to the minor empirical refinement of the equilibrium Si–H bond length.

E. Overview of rotation-vibration spectrum

As a final test of the PES and DMS, in Fig. 3 we have simulated the rotation-vibration spectrum of ^{28}SiH$_4$ for transitions up to $J = 20$ at 296 K. A polyad number of P_{max} = 10 was employed. Transition frequencies and corresponding intensities were calculated for a 5000 cm^{-1} frequency window with a lower state energy threshold of 5000 cm^{-1}. To simulate the spectrum a Gaussian profile with a half width at half maximum of 0.135 cm^{-1} was chosen as this appears to closely match the line shape used by the PNNL spectral library.[35] The experimental PNNL silane spectrum, also shown in Fig. 3, is at a resolution of around 0.06 cm^{-1}. It was measured at a temperature of 25 °C with the dataset subsequently re-
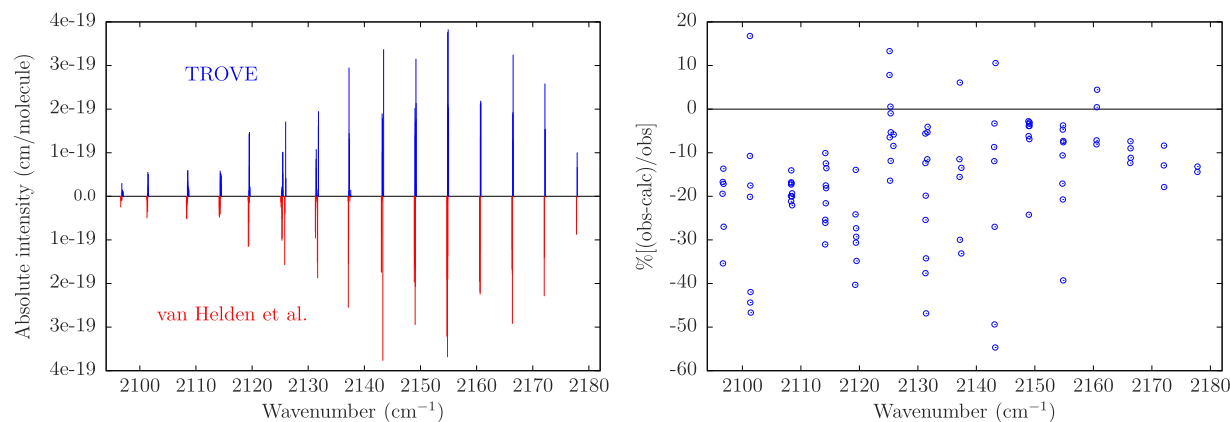
FIG. 2. Absolute line intensities of the ν_3 band for transitions up to $J = 16$ (left) and the corresponding residuals $\left(\% \left[\frac{\text{obs}-\text{calc}}{\text{obs}}\right]\right)$ (right) when compared with measurements from van Helden *et al.*[89]
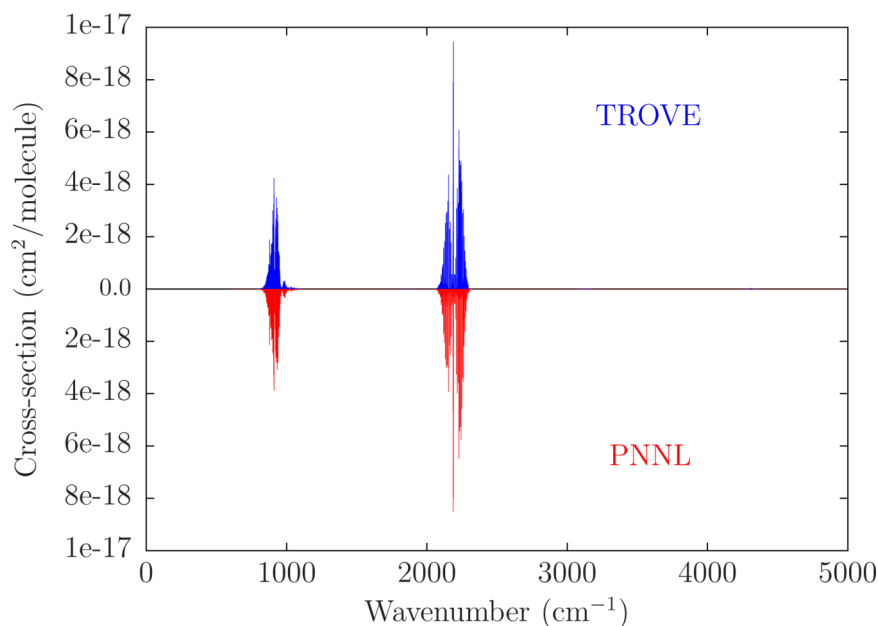

FIG. 3. Overview of simulated ^{28}SiH$_4$ rotation-vibration spectrum up to $J = 20$. Note that the experimental PNNL spectrum[35] is composed of ^{28}SiH$_4$ (92.2%), ^{29}SiH$_4$ (4.7%), and ^{30}SiH$_4$ (3.1%) (see text).
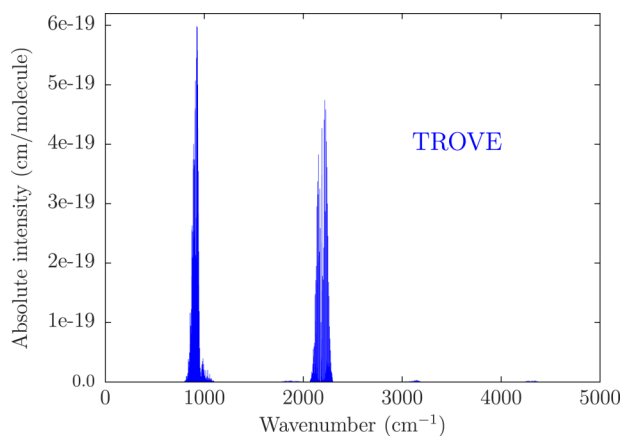
FIG. 4. Overview of absolute line intensities of ^{28}SiH$_4$ up to $J = 20$.

normalized to 22.84 °C (296 K). Note that the PNNL spectrum is of electronics grade silane gas which is composed of ^{28}SiH$_4$ (92.2%), ^{29}SiH$_4$ (4.7%), and ^{30}SiH$_4$ (3.1%). We have therefore scaled the TROVE computed ^{28}SiH$_4$ cross-sections by 0.922 to provide a reliable comparison.

The computed TROVE intensities are marginally stronger but overall there is good agreement with the experimental PNNL results. Even with $P_{\text{max}} = 10$ which does not give fully converged transition frequencies both band shape and position appear reliable. Of course there are shortcomings in our simulations which we will now discuss.

Some of the band structure is undoubtedly lost as we have not considered ^{29}SiH$_4$ or ^{30}SiH$_4$, and by only computing transitions up to $J = 20$ the spectrum is unlikely to be complete at room temperature. There may also be minor errors arising from the use of a Gaussian profile to model the line shape. More desirable would be to fit a Voigt profile which incorporates instrumental factors. The largest source of error, as discussed before, is likely to be the electronic structure calculations. For the purposes of modelling exoplanet atmospheres however, we expect that the level of theory employed to compute the DMS is sufficient. The features of the SiH$_4$ spectrum are clear and identifiable as seen in Fig. 3.

Note that in Fig. 3 the ν_3 (2189.19 cm^{-1}) band is stronger than the ν_4 (913.47 cm^{-1}) band. This is contrast to the vibrational transition moments where $\mu_{\nu_4} > \mu_{\nu_3}$. If, however,

we plot absolute line intensities up to $J = 20$ as shown in Fig. 4, the ν_4 band is indeed stronger than the ν_3 band. The behaviour displayed in Fig. 3 is caused by the use of a line profile to model the spectrum.

V. CONCLUSIONS

High-level *ab initio* theory has been used to generate global potential energy and dipole moment surfaces for silane. The quality of the PES is reflected by the achievement of sub-wavenumber accuracy for all four fundamental frequencies. Combination and overtone bands are also consistently reproduced which confirms that the level of *ab initio* theory used to generate the PES is adequate. Minor empirical refinement of the equilibrium geometry of SiH_4 produced a Si–H bond length in excellent agreement with previous experimental and theoretical results. The rotational structure of vibrational bands was improved as a result of the refinement. Ultimately though, to achieve sub-wavenumber accuracy for all rotation-vibration energy levels, a rigorous empirical refinement of the PES is necessary.[90]

A new *ab initio* DMS has been computed and utilized to simulate the infrared spectrum of SiH_4. Absolute line intensities are marginally overestimated and we suspect this behaviour can be resolved by using a larger basis set for the electronic structure calculations when computing the DMS. Overall however, band shape and structure across the spectrum display good agreement with experiment. The PES and DMS presented in this work will be used to compute a comprehensive rovibrational line list applicable for elevated temperatures as part of the ExoMol project.[29]

ACKNOWLEDGMENTS

[1] W. B. Steward and H. H. Nielsen, J. Chem. Phys. **2**, 712 (1934).
[2] W. B. Steward and H. H. Nielsen, Phys. Rev. **47**, 828 (1935).
[3] D. M. Goldhaber and A. L. Betz, Astrophys. J. **279**, L55 (1984).
[4] J. J. Keady and S. T. Ridgway, Astrophys. J. **406**, 199 (1993).
[5] J. D. Monnier, W. C. Danchi, D. S. Hale, P. G. Tuthill, and C. H. Townes, Astrophys. J. **543**, 868 (2000).
[6] R. R. Treffers, H. P. Larson, U. Fink, and T. N. Gautier, Icarus **34**, 331 (1978).
[7] H. P. Larson, U. Fink, H. A. Smith, and D. S. Davis, Astrophys. J. **240**, 327 (1980).
[8] J. M. L. Martin, K. K. Baldridge, and T. J. Lee, Mol. Phys. **97**, 945 (1999).
[9] T. H. Dunning, Jr., J. Chem. Phys. **90**, 1007 (1989).
[10] J. M. L. Martin and O. Uzan, Chem. Phys. Lett. **282**, 16 (1998).
[11] X. G. Wang and E. L. Sibert, J. Chem. Phys. **113**, 5384 (2000).
[12] X. W. Hou, F. Borondo, and R. M. Benito, Chem. Phys. Lett. **344**, 421 (2001).
[13] L. Halonen and M. S. Child, Mol. Phys. **46**, 239 (1982).
[14] L. Halonen and M. S. Child, Comput. Phys. Commun. **51**, 173 (1988).
[15] D. Permogorov and A. Campargue, Mol. Phys. **92**, 117 (1997).
[16] J. K. Xie and J. Tennyson, Mol. Phys. **100**, 1615 (2002).
[17] H. Lin, D. Wang, X. Y. Chen, X. G. Wang, Z. P. Zhou, and Q. S. Zhu, J. Mol. Spectrosc. **192**, 249 (1998).
[18] H. Lin, L. F. Yuan, and Q. S. Zhu, Chem. Phys. Lett. **308**, 137 (1999).
[19] H. Lin, S. G. He, X. G. Wang, L. F. Yuan, H. Bürger, J. F. D'Eu, N. Reuter, and W. Thiel, Phys. Chem. Chem. Phys. **3**, 3506 (2001).
[20] S. G. He, A. W. Liu, H. Lin, S. M. Hu, J. J. Zheng, L. Y. Hao, and Q. S. Zhu, J. Chem. Phys. **117**, 10073 (2002).
[21] Q. S. Zhu, B. S. Zhang, Y. R. Ma, and H. B. Qian, Chem. Phys. Lett. **164**, 596 (1989).
[22] Q. S. Zhu, B. S. Zhang, Y. R. Ma, and H. B. Qian, Spectrochim. Acta, Part A **46**, 1217 (1990).
[23] Q. S. Zhu, H. Ma, B. S. Zhang, Y. R. Ma, and H. B. Qian, Spectrochim. Acta, Part A **46**, 1323 (1990).
[24] Q. S. Zhu, H. B. Qian, H. Ma, and L. Halonen, Chem. Phys. Lett. **177**, 261 (1991).
[25] F. G. Sun, X. G. Wang, Q. S. Zhu, C. Pierre, and G. Pierre, Chem. Phys. Lett. **239**, 373 (1995).
[26] Q. S. Zhu, A. Campargue, and F. Stoeckel, Spectrochim. Acta, Part A **50**, 663 (1994).
[27] H. Lin, H. Bürger, S. G. He, L. F. Yuan, J. Breidung, and W. Thiel, J. Phys. Chem. A **105**, 6065 (2001).
[28] S. N. Yurchenko, *Chemical Modelling: Volume 10* (The Royal Society of Chemistry, 2014), Vol. 10, pp. 183–228.
[29] J. Tennyson and S. N. Yurchenko, Mon. Not. R. Astron. Soc. **425**, 21 (2012).
[30] S. Seager, W. Bains, and R. Hu, Astrophys. J. **777**, 95 (2013).
[31] L. Rothman, I. Gordon, Y. Babikov, A. Barbe, D. C. Benner, P. Bernath, M. Birk, L. Bizzocchi, V. Boudon, L. Brown, A. Campargue, K. Chance, E. Cohen, L. Coudert, B. Devi, B. Drouin, A. Fayt, J.-M. Flaud, R. Gamache, J. Harrison, J.-M. Hartmann, C. Hill, J. Hodges, D. Jacquemart, A. Jolly, J. Lamouroux, R. L. Roy, G. Li, D. Long, O. Lyulin, C. Mackie, S. Massie, S. Mikhailenko, H. Müller, O. Naumenko, A. Nikitin, J. Orphal, V. Perevalov, A. Perrin, E. Polovtseva, C. Richard, M. Smith, E. Starikova, K. Sung, S. Tashkun, J. Tennyson, G. Toon, V. Tyuterev, and G. Wagner, J. Quant. Spectrosc. Radiat. Transf. **130**, 4 (2013).
[32] N. Jacquinet-Husson, L. Crepeau, R. Armante, C. Boutammine, A. Chédin, N. A. Scott, C. Crevoisier, V. Capelle, C. Boone, N. Poulet-Crovisier, A. Barbe, A. Campargue, D. C. Benner, Y. Benilan, B. Bézard, V. Boudon, L. R. Brown, L. H. Coudert, A. Coustenis, V. Dana, V. M. Devi, S. Fally, A. Fayt, J. M. Flaud, A. Goldman, M. Herman, G. J. Harris, D. Jacquemart, A. Jolly, I. Kleiner, A. Kleinboehl, F. Kwabia-Tchana, N. Lavrentieva, N. Lacome, L.-H. Xu, O. M. Lyulin, J. Y. Mandin, A. Maki, S. Mikhailenko, C. E. Miller, T. Mishina, N. Moazzen-Ahmadi, H. S. P. Müller, A. Nikitin, J. Orphal, V. Perevalov, A. Perrin, D. T. Petkie, A. Predoi-Cross, C. P. Rinsland, J. J. Remedios, M. Rotger, M. A. H. Smith, K. Sung, S. Tashkun, J. Tennyson, R. A. Toth, A. C. Vandaele, and J. Vander Auwera, J. Quant. Spectrosc. Radiat. Transf. **112**, 2395 (2011).
[33] H. M. Pickett, R. L. Poynter, E. A. Cohen, M. L. Delitsky, J. C. Pearson, and H. S. P. Müller, J. Quant. Spectrosc. Radiat. Transf. **60**, 883 (1998).
[34] H. S. P. Müller, F. Schlöder, J. Stutzki, and G. Winnewisser, J. Mol. Struct. **742**, 215 (2005).
[35] S. W. Sharpe, T. J. Johnson, R. L. Sams, P. M. Chu, G. C. Rhoderick, and P. A. Johnson, Appl. Spectrosc. **58**, 1452 (2004).
[36] C. Wenger and J. P. Champion, J. Quant. Spectrosc. Radiat. Transf. **59**, 471 (1998).
[37] A. G. Császár, W. D. Allen, and H. F. Schaefer III, J. Chem. Phys. **108**, 9751 (1998).
[38] T. B. Adler, G. Knizia, and H.-J. Werner, J. Chem. Phys. **127**, 221106 (2007).
[39] K. A. Peterson, T. B. Adler, and H.-J. Werner, J. Chem. Phys. **128**, 084102 (2008).
[40] S. Ten-No, Chem. Phys. Lett. **398**, 56 (2004).
[41] J. G. Hill, K. A. Peterson, G. Knizia, and H.-J. Werner, J. Chem. Phys. **131**, 194105 (2009).
[42] K. E. Yousaf and K. A. Peterson, J. Chem. Phys. **129**, 184108 (2008).
[43] F. Weigend, Phys. Chem. Chem. Phys. **4**, 4285 (2002).
[44] C. Hättig, Phys. Chem. Chem. Phys. **7**, 59 (2005).
[45] H.-J. Werner, P. J. Knowles, G. Knizia, F. R. Manby, and M. Schuetz, Comput. Mol. Sci. **2**, 242 (2012).
[46] M. Douglas and N. M. Kroll, Ann. Phys. **82**, 89 (1974).
[47] B. A. Heß, Phys. Rev. A **33**, 3742 (1986).
[48] W. A. de Jong, R. J. Harrison, and D. A. Dixon, J. Chem. Phys. **114**, 48 (2001).
[49] G. Tarczay, A. G. Császár, W. Klopper, and H. M. Quiney, Mol. Phys. **99**, 1769 (2001).
[50] J. G. Hill, S. Mazumder, and K. A. Peterson, J. Chem. Phys. **132**, 054108 (2010).
[51] M. Kállay and J. Gauss, J. Chem. Phys. **123**, 214105 (2005).
[52] M. Kállay and J. Gauss, J. Chem. Phys. **129**, 144101 (2008).
[53] MRCC, A string-based quantum chemical program suite written by M. Kállay, See also, M. Kállay and P. R. Surján, J. Chem. Phys. **115**, 2945 (2001), as well as www.mrcc.hu.

[54] CFOUR, A quantum chemical program package written by J. F. Stanton, J. Gauss, M. E. Harding, and P. G. Szalay with contributions from A. A. Auer, R. J. Bartlett, U. Benedikt, C. Berger, D. E. Bernholdt, Y. J. Bomble, L. Cheng, O. Christiansen, M. Heckert, O. Heun, C. Huber, T.-C. Jagau, D. Jonsson, J. Jusélius, K. Klein, W. J. Lauderdale, D. A. Matthews, T. Metzroth, L. A. Mück, D. P. O'Neill, D. R. Price, E. Prochnow, C. Puzzarini, K. Ruud, F. Schiffmann, W. Schwalbach, S. Stopkowicz, A. Tajti, J. Vázquez, F. Wang, J. D. Watts, and the integral packages MOLECULE (J. Almlöf and P. R. Taylor), PROPS (P. R. Taylor), ABACUS (T. Helgaker, H. J. Aa. Jensen, P. Jørgensen, and J. Olsen), and ECP routines by A. V. Mitin and C. van Wüllen. For the current version, see http://www.cfour.de.

[55] R. A. Kendall, T. H. Dunning, Jr., and R. J. Harrison, J. Chem. Phys. **96**, 6796 (1992).

[56] D. E. Woon and T. H. Dunning, Jr., J. Chem. Phys. **98**, 1358 (1993).

[57] T. H. Dunning, Jr., K. A. Peterson, and A. K. Wilson, J. Chem. Phys. **114**, 9244 (2001).

[58] J. Gauss, A. Tajti, M. Kállay, J. F. Stanton, and P. G. Szalay, J. Chem. Phys. **125**, 144111 (2006).

[59] A. Yachmenev, S. N. Yurchenko, T. Ribeyre, and W. Thiel, J. Chem. Phys. **135**, 074302 (2011).

[60] A. Owens, S. N. Yurchenko, A. Yachmenev, J. Tennyson, and W. Thiel, J. Chem. Phys. **142**, 244306 (2015).

[61] S. N. Yurchenko, J. Tennyson, R. J. Barber, and W. Thiel, J. Mol. Spectrosc. **291**, 69 (2013).

[62] S. N. Yurchenko and J. Tennyson, Mon. Not. R. Astron. Soc. **440**, 1649 (2014).

[63] S. N. Yurchenko, J. Tennyson, J. Bailey, M. D. J. Hollis, and G. Tinetti, Proc. Natl. Acad. Sci. U. S. A. **111**, 9379 (2014).

[64] P. R. Bunker and P. Jensen, *Molecular Symmetry and Spectroscopy*, 2nd ed. (NRC Research Press, Ottawa, 1998).

[65] H. Partridge and D. W. Schwenke, J. Chem. Phys. **106**, 4618 (1997).

[66] J. K. G. Watson, J. Mol. Spectrosc. **219**, 326 (2003).

[67] T. J. Lee and P. R. Taylor, Int. J. Quant. Chem. **36**, 199 (1989).

[68] See supplementary material at http://dx.doi.org/10.1063/1.4938563 for the parameters of the potential energy surface and dipole moment surface for SiH$_4$.

[69] S. N. Yurchenko, R. J. Barber, A. Yachmenev, W. Thiel, P. Jensen, and J. Tennyson, J. Phys. Chem. A **113**, 11845 (2009).

[70] A. Yachmenev, I. Polyak, and W. Thiel, J. Chem. Phys. **139**, 204308 (2013).

[71] K. Ohno, H. Matsuura, Y. Endo, and E. Hirota, J. Mol. Spectrosc. **111**, 73 (1985).

[72] S. Coriani, D. Marchesan, J. Gauss, C. Hättig, T. Helgaker, and P. Jørgensen, J. Chem. Phys. **123**, 184107 (2005).

[73] S. N. Yurchenko, W. Thiel, and P. Jensen, J. Mol. Spectrosc. **245**, 126 (2007).

[74] A. Yachmenev and S. N. Yurchenko, J. Chem. Phys. **143**, 014105 (2015).

[75] B. V. Noumerov, Mon. Not. R. Astron. Soc. **84**, 592 (1924).

[76] J. W. Cooley, Math. Comput. **15**, 363 (1961).

[77] R. I. Ovsyannikov, W. Thiel, S. N. Yurchenko, M. Carvajal, and P. Jensen, J. Chem. Phys. **129**, 044309 (2008).

[78] M. Chevalier, Thesis, Université de Paris Sud, France, 1988.

[79] R. A. Bernheim, F. W. Lampe, J. F. O'Keefe, and J. R. Qualey III, J. Chem. Phys. **80**, 5906 (1984).

[80] K. Fox and W. B. Person, J. Chem. Phys. **64**, 5218 (1976).

[81] D. F. Ball and D. C. McKean, Spectrochim. Acta **18**, 1019 (1962).

[82] I. W. Levin and W. T. King, J. Chem. Phys. **37**, 1375 (1962).

[83] A. M. Coats, D. C. McKean, and D. Steele, J. Mol. Struct. **320**, 269 (1994).

[84] J. Cadot, J. Mol. Spectrosc. **154**, 383 (1992).

[85] K. Fox, J. Quant. Spectrosc. Radiat. Transf. **10**, 1335 (1970).

[86] M. Dang-Nhu, G. Pierre, and R. Saint-Loup, Mol. Phys. **28**, 447 (1974).

[87] G. Pierre, G. Guelachvili, and C. Amiot, J. Phys. France **36**, 487 (1975).

[88] G. Pierre, A. Valentin, and L. Henry, Can. J. Phys. **62**, 254 (1984).

[89] J. H. van Helden, D. Lopatik, A. Nave, N. Lang, P. B. Davies, and J. Röpcke, J. Quant. Spectrosc. Radiat. Transf. **151**, 287 (2015).

[90] S. N. Yurchenko, R. J. Barber, J. Tennyson, W. Thiel, and P. Jensen, J. Mol. Spectrosc. **268**, 123 (2011).